Journal of Marine Science and Application (2025) 24: 1194-1207
https://doi.org/10.1007/s11804-025-00654-z

RESEARCH ARTICLE

Coupling Actions Between Ship Roll Motion and Internal Sloshing with Water and LNG Inside

Zihao Wang[1], YunHe Wang[2] and Shengchao Jiang[1,2]

Received: 13 September 2024 / Accepted: 23 November 2024
© Harbin Engineering University and Springer-Verlag GmbH Germany, part of Springer Nature 2025

Abstract

The coupling effect between ship motion and liquid sloshing in a beam sea is investigated, with a focus on the influence of liquid types, namely, water and liquefied natural gas (LNG), on the coupling dynamics. A hybrid numerical model, combining a potential flow model and computational fluid dynamics methods, is employed to simulate these interactions. Numerical validation is performed using experimental data from water sloshing tests. Comparisons between water and LNG reveal that liquid type has minimal effects on the ship's roll motion response in a beam sea, provided the total liquid masses are the same. Regarding sloshing impact pressure, although differences between LNG and water results are minor, substituting LNG with water in physical experiments is shown to yield reliable results.

Keywords LNG carrier; LNG and water; Roll motion; Coupling sloshing; Local pressure

1 Introduction

With the increasing scarcity of land-based natural gas resources in recent years, demand has outpaced supply, driving international interest in offshore natural gas development. The safety and reliability of liquefied natural gas (LNG) carriers and floating liquefied natural gas (FLNGs), essential for LNG production and transportation, have attracted considerable attention. Partial filling of tanks is inevitable during production, loading, transportation, and offloading. Under such conditions, external wave action induces ship motion, leading to internal sloshing within the tanks. This sloshing, in turn, influences the ship's motion, highlighting the coupling effect between ship motion and liquid sloshing. This coupling effect is especially pronounced in ship roll motion. When the external wave period aligns with the natural periods of ship motion and sloshing, violent resonance can occur. This condition not only degrades ship motion performance but also generates great impact pressure on tank walls. Consequently, the study of LNG tank sloshing and its coupling effects on ship motion has critical engineering importance.

Numerical simulations and physical model experiments have been adopted to investigate the coupling between ship motion and liquid sloshing. Most early numerical simulations, such as Molin (2002), Chen (2004), Gaillarde et al. (2004), and Newman (2005), were conducted based on linear potential flow theory in the frequency domain. These studies modeled the internal sloshing effects as added mass, added damping, and restoring force, allowing the sloshing effects on the ship motion to be considered, such as Molin (2002), Chen (2004), Gaillarde et al. (2004) and Newman (2005). However, due to the strongly nonlinear nature of liquid sloshing, linear potential flow models cannot accurately capture its behavior. With advances in computer performance and the development of computational fluid dynamics (CFD) methods, full-time domain numerical models have been used to simulate ship motion coupled with sloshing. Bouscasse et al. (2013) developed a weakly compressible SPH model, whereas Wang et al. (2017) used a time-domain boundary element method to simulate the motion of a 2D tank coupled with sloshing under wave action. Cao et al. (2019), Zhuang and Wan (2019), and Huang et al. (2021) highlighted the considerable nonlinear influences of sloshing on ship motion, especially in scenarios involving ship damage and varying fill levels. Liu et al. (2022) employed CFD methods to exam-

Article Highlights

- A hybrid numerical method is used to investigate the coupling effect between ship motion and liquid sloshing.
- Water can be reliably substituted for LNG in beam wave experiments investigating the motion response of LNG ships.
- Sloshing impact pressures of water and LNG-filled liquid tanks maintain an overall relationship of ρ_{LNG}/ρ_{water}.

✉ Shengchao Jiang
jiangshengchao@foxmail.com

[1] School of Naval Architecture and Ocean Engineering, Dalian University of Technology, Dalian 116024, China

[2] State Key Laboratory of Coastal and Offshore Engineering, Dalian University of Technology, Dalian 116024, China

ine the coupling between parametric roll motion and sloshing in ships with forward speed. Jiao et al. (2024a, 2024b) used the SPH method to simulate the interaction of tank sloshing with the motion of a single LNG carrier and two side-by-side ships. Zhao et al. (2024) applied CFD methods to investigate the motion response of a cylindrical floating production storage and offloading system coupled with sloshing under regular wave conditions. Full-time domain numerical methods require substantial computational effort with suboptimal efficiency. Ship motion under wave action is a classical hydrodynamic problem that can be effectively addressed using simpler numerical models. By contrast, sloshing involves highly nonlinear fluid motion, requiring more accurate numerical approaches. Therefore, hybrid numerical methods have been developed, distinct models for external wave and internal sloshing. Coupling strategies mainly include the impulsive response function method, used by Lee and Kim (2010), Li et al. (2019), Jiang and Bai (2020), and Lyu et al. (2022), and the time-domain Green function method, applied by Huang et al. (2018), Saripilli and Sen (2018), and Zhuang et al. (2022).

Physical experimental measurement is another effective approach for studying the coupling between ship motion and liquid sloshing. Rognebakke and Faltinsen (2003) conducted 2D experiments to investigate the coupling between ship sway motion and liquid sloshing, demonstrating a significant interaction between the two. Nam et al. (2009) performed physical experiments on the coupling of three degrees of freedom motion and liquid sloshing in an LNG/FPSO under wave action, highlighting the critical role of sloshing nonlinearity in the coupling effects. Tabri et al. (2009) examined the effects of sloshing during ship collisions using experimental methods. Their findings attributed the sloshing effect to delayed momentum transfer, suggesting that liquid loading reduces collision damage by effectively making the ship lighter. Zhao et al. (2014a, 2014b) investigated the interaction between FLNG section motion responses and liquid sloshing through 2D experiments. The most significant effect of sloshing occurs on ship roll motion, primarily due to the first mode of sloshing. Hu et al. (2017) conducted experiments on the influence of sloshing on the motion response of an FLNG system. Su and Liu (2017) carried out physical experiments on a rectangular barge coupled with liquid sloshing, revealing that the coupling effect is most pronounced when the natural frequency of the barge's roll motion aligns with the first-order sloshing mode. Zhao et al. (2018) modeled the nonlinearity of ship roll motion with and without sloshing under irregular wave action. A four-phase approach based on weak nonlinearity theory was implemented to extract the components of irregular high-frequency signals coupled with low-frequency signals. Their study revealed that, although internal sloshing is nonlinear, the coupling effects of sloshing on roll motion behave as linear interactions. Zhu et al. (2021) investigated the influence of the coupling effect between sloshing and ship motion on total ship resistance through experiments. They found that internal sloshing greatly affects surge motion, with the effect varying depending on the filling ratio. Zheng et al. (2021) experimentally investigated the interaction between ship motion and liquid sloshing on added wave resistance. They found that internal sloshing reduced the added resistance and, consequently, the energy dissipation of the ship at 70% filling condition. He et al. (2022) compared the motion of a ship with and without an internal liquid tank under beam wave action through experiments. They showed that internal sloshing increased roll motion when the wavelength ratio was small but suppressed roll motion when the wavelength ratio was large. Zhang et al. (2023) experimentally studied the heave and pitch motion responses of a floating body with internal liquid sloshing under regular wave action.

However, these experimental studies used water to simulate liquid sloshing, though LNG is used in practical engineering. The use of water as an alternative has become the most popular method in experimental measurement because finding a liquid with the same properties as LNG under normal temperatures and pressures. Nevertheless, does this approach provide sufficient accuracy? Unfortunately, comparative analyses on the coupling sloshing problem between water and LNG are limited. In this study, a hybrid numerical model is employed to conduct a series of simulations for ships with different filling depths and liquid types in a beam sea. The validity of replacing LNG with water is discussed in terms of ship motion response and internal sloshing pressure.

2 Experimental and numerical simulation description

2.1 Experimental settings

The physical experiments were conducted in the Ship Model Towing Tank at Dalian University of Technology, as shown in Figure 1. The towing tank is 170 m long, 7 m wide, with a water depth of 3.65 m. Regular waves are generated on one side of the tank by a wave maker consisting of 20 electrical swing-type paddles, and wave absorbers are installed on the opposite side to minimize wave reflections. The LNG carrier with two prismatic tanks is shown in Figure 1(b). Note that the middle tank is empty in the experiments presented in this paper. The model scale is 1:50, and the basic parameters of the ship model are shown in Table 1. The prismatic tanks are made of plexiglass, with the arrangement and specific details of the two tanks shown in Figures 2 and 3. In the experiments, the liquid in the tanks is water.

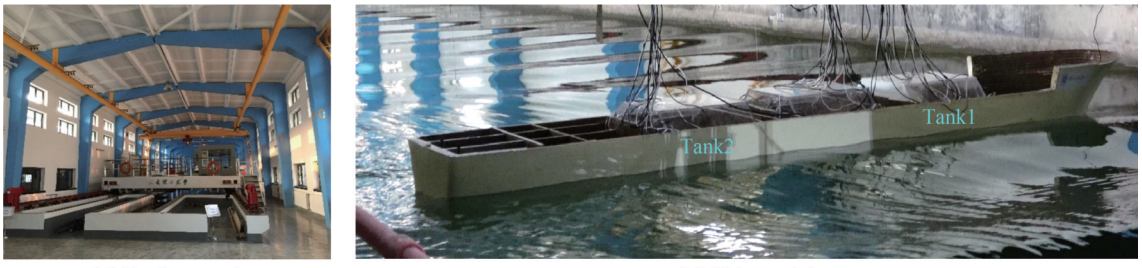

(a) Environment (b) Ship model

Figure 1 Experimental environment and ship model arrangement

Table 1 Basic parameters of the ship model without liquid tanks

Main parameters	Draft D (m)		
	0.12	0.16	0.21
Length over all L (m)	-	4.360	-
Molded breath B (m)	-	0.660	-
Molded depth D (m)	-	0.360	-
Displacement $\triangle$ (t)	0.290	0.390	0.530
Height of center of gravity KG (m)	0.138	0.133	0.125
Transverse metacenter GM (m)	0.182	0.135	0.122
Rolling radius of gyration k_{xx} (m)	0.197	0.196	0.196
Pitching radius of gyration k_{yy} (m)	1.470	1.330	1.730
Yawing radius of gyration k_{zz} (m)	1.650	1.330	1.170

The experiments included three filling depths: 20%, 40%, and 60%, corresponding to drafts of 0.12, 0.16, and 0.21 m in Table 1, respectively. The regular wave amplitude is A_i = 0.025 m, and the incident wave periods range from 0.85 s to 2.00 s. During the experiments, the ship model was connected to a stationary towing carriage through a horizontal mooring system. This mooring system was designed to prevent the model from drifting while minimizing any significant constraints on the ship's natural roll periods. The beam sea condition was tested in this study. The ship's roll motion was monitored using an Innalabs® attitude and heading reference system, with a measurement accuracy of 0.04° and a sampling frequency of 50 Hz.

2.2 Numerical modeling principles

Two coordinate systems are defined, as shown in Figure 4: the ship-fixed coordinate system (XYZ) and the tank-fixed coordinate system (xyz). The ship-fixed coordinate system is used to describe the ship's motion, whereas the tank-fixed coordinate system is used to describe the internal sloshing flow.

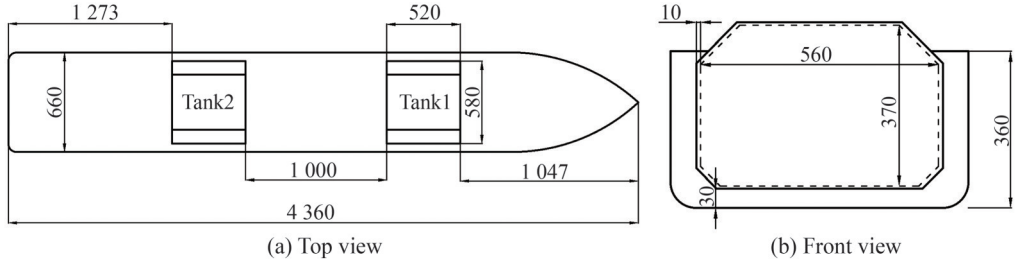

(a) Top view (b) Front view

Figure 2 Schematic layout of the experimental tanks (unit: mm)

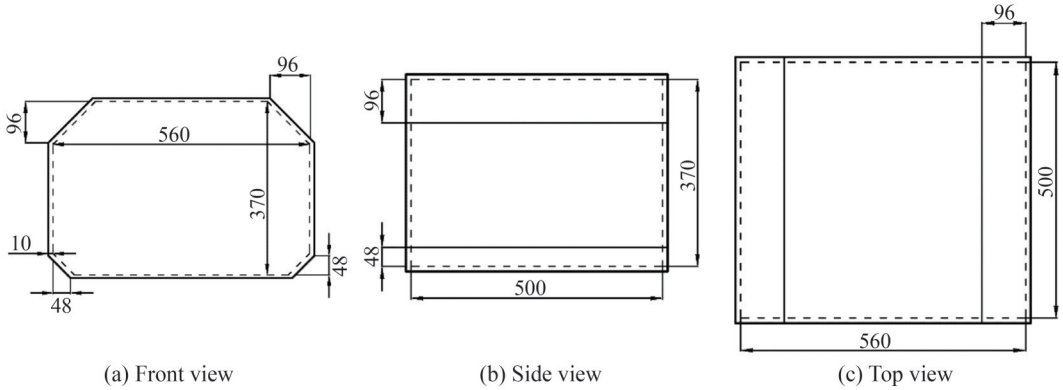

(a) Front view (b) Side view (c) Top view

Figure 3 Experimental tank dimensions (unit: mm)

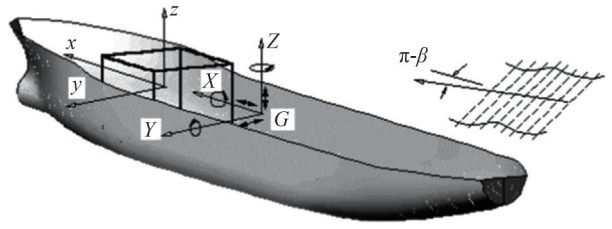

Figure 4 Coordinate system for ship model with liquid tanks

The default earth-fixed or space-fixed coordinate system is used to describe the external fluid flow and coupling strategy.

A linear potential flow model with the Laplace equation as the governing equation in the frequency domain is used to calculate the external wave action. A viscous fluid flow model is applied to describe the internal sloshing flow. The coupling of internal sloshing and external waves is achieved through the motion equations of a floating body, based on Newton's second law. The ship motion equations can be formulated as follows:

$$\left[M_{ij} + a_{ij}^{\text{ext}}(\infty)\right]\ddot{\zeta}_j(t) + B_{ij}^{\text{vis}}\dot{\zeta}_j(t) + \int_0^t R_{ij}^{\text{ext}}(t-\tau)\dot{\zeta}_j(\tau)\mathrm{d}\tau = F_j^{\text{ext}}(t) + F_j^{\text{int}}(t) \quad (1)$$

where $j = 1, 2, \cdots, 6$, represents the ship motion in six degrees of freedom. $\zeta_j(t)$ indicates the ship motion response, and in particular, $\zeta_4(t)$ denotes the ship roll motion. The superscript "int" refers to parameters related to internal sloshing, whereas "ext" refers to parameters related to external wave action on the ship. M_{ij} indicates the ship's mass, excluding the mass of the fluid in the tank, and B_{ij}^{vis} denotes the viscous damping coefficient, which can be estimated from linear damping (Nam et al., 2009; Gou et al., 2011). $a_{ij}^{\text{ext}}(\infty)$, $R_{ij}^{\text{ext}}(t)$, and $F_j^{\text{ext}}(t)$ represent the added mass at infinite frequency, the retardation function, and the external wave exciting force, respectively. As shown in Figure 4, the incident wave potential of a ship moving in a wave is as follows:

$$\phi_I = \frac{gA}{\omega}\mathrm{Re}\left[\exp\left\{\mathrm{i}k\left(x\cos\beta + y\sin\beta\right) - \mathrm{i}\left(\omega t + \varphi\right) + kz\right\}\right] \quad (2)$$

where $g = 9.81$ m/s^2 indicates the gravitational acceleration, and A and ω represent the wave amplitude and wave frequency, respectively. k, β, and φ denote the wave number, heading angle, and phase shift, respectively. The added mass $a_{ij}(\omega)$, radiation damping $b_{ij}(\omega)$, and exciting force $H_i(\omega)$ in the frequency domain can be calculated using the higher-order boundary element method (Teng and Eatock Taylor, 1995) based on classical first-order diffraction/radiation potential theory.

Based on the frequency domain results, the hydrodynamic parameters $a_{ij}^{\text{ext}}(\infty)$, $R_{ij}^{\text{ext}}(t)$, and $F_j^{\text{ext}}(t)$ of the external wave in the time domain of the ship-motion equations can be derived using the IRF method. The retardation function can be obtained by performing Fourier integration of the frequency domain radiation damping as follows:

$$R_{ij}^{\text{ext}}(t) = \frac{2}{\pi}\int_0^\infty b_{ij}(\omega)\cos(\omega t)\mathrm{d}\omega \quad (3)$$

For the added mass, the time and frequency domain conversion relations according to the IRF are as follows:

$$a_{ij}^{\text{ext}}(\infty) = a_{ij}(\omega) + \frac{1}{\omega}\int_0^\infty R_{ij}(t)\sin(\omega t)\mathrm{d}t \quad (4)$$

Similar to the added mass and retardation functions, the wave exciting force on the ship can be calculated as follows:

$$F_i^{\text{ext}}(t) = \int_0^t h_i(t-\tau)\eta(\tau)\mathrm{d}\tau \quad (5)$$

where $\eta(t)$ indicates the elevation of the incident wave, and $h_i(t)$ represents the response per unit impulse input, which is the impulse response function; it can be calculated using the frequency domain excitation force according to Fourier transformation, as follows:

$$h_i(t) = \Re\left[\frac{1}{\pi}\int_0^\infty H_i(\omega)\mathrm{e}^{-\mathrm{i}\omega t}\mathrm{d}t\right] \quad (6)$$

A more detailed formula is presented in Cummins (1962).

$F_j^{\text{int}}(t)$ in Equation (1) indicates the internal fluid force, including sloshing and hydrostatic forces, computed using a viscous numerical model based on the Navier-Stokes equations in the Arbitrary Lagrangian–Eulerian (ALE) reference system, as follows:

$$\frac{\partial \rho u_i}{\partial x_i} = 0 \quad (7)$$

$$\frac{\partial \rho u_i}{\partial t} + \frac{\partial \rho\left(u_j - u_j^m\right)u_i}{\partial x_j} = \rho g - \frac{\partial p}{\partial x_i} + \mu\frac{\partial}{\partial x_j}\left(\frac{\partial u_i}{\partial x_j} + \frac{\partial u_j}{\partial x_i}\right) \quad (8)$$

where ρ, p, and μ represent the internal liquid density, pressure, and dynamic viscosity, respectively. u_i refers to the component of velocity in the ith direction, and u_j^m indicates the component of velocity due to mesh deformation. In this study, internal sloshing is simulated using the OpenFOAM® software package. The free surface of the internal fluid is modeled using the volume of fluid method to capture nonlinear phenomena such as breaking and overturning. In this method, the fraction indicator α is defined as follows:

$$\alpha = \begin{cases} \alpha = 0, & \text{in air} \\ 0 < \alpha < 1, & \text{in free surface} \\ \alpha = 1, & \text{in water} \end{cases} \quad (9)$$

Its distribution obeys the following advection equation:

$$\frac{\partial \alpha}{\partial t} + \frac{\partial\left(\alpha\left(u_i - u_i^m\right)\right)}{\partial x_i} + \frac{\partial\left(\alpha(1-\alpha)u_i^r\right)}{\partial x_i} = 0 \quad (10)$$

where u_i^r represents the relative velocity between air and water. The last term on the left of Equation (10) is used for compression, which can restrict the diffusion of the free surface. According to the fractional index α in the cell, the fluid dynamic viscosity and density can be calculated as follows:

$$\mu = \varphi\mu_w + (1-\varphi)\mu_a, \rho = \varphi\rho_w + (1-\varphi)\rho_a \quad (11)$$

where subscript w refers to water, and a indicates air. In numerical computations, the free surface elevation is represented by the $\alpha = 0.5$ contour. The interFOAM solver, based on the finite volume method in OpenFOAM®, is used to simulate the motion of the two-phase flow interface. The pressure–velocity coupling is solved using the PISO-SIMPLE (PIMPLE) algorithm. The boundary conditions in the calculations include no-slip and moving-wall conditions.

The coupling strategy for external waves and internal sloshing is illustrated in Figure 5 and consists of three components: external wave action, internal sloshing action, and coupling analysis. The wave action involves the computation of the added mass $a_{ij}^{\text{ext}}(\infty)$, the retardation function $R_{ij}^{\text{ext}}(t)$, and the wave exciting force $F_j^{\text{ext}}(t)$. Sloshing in the tank is computed using the CFD method to determine the internal fluid force $F_j^{\text{int}}(t)$. Then, the ship motion response is obtained by solving Equation (1), completing the coupled analysis of the internal and external flow fields. The ship motion response is applied as the moving-wall boundary condition for the next time step of the sloshing simulation. To ensure the accuracy of the internal sloshing simulation, the adaptive time step is determined according to the following CFL conditions:

$$\Delta t \leqslant C_r \times \min\left\{\sqrt{S_e}/|u_e|\right\} \quad (12)$$

where $|u_e|$ denotes the absolute velocity of the computational cell and S_e is its area. The Courant number C_r is usually less than or equal to 1.0. In this simulation, $C_r = 0.2$ is used to ensure the stability of the computation. The B-spline interpolation method is employed to deal with the retardation function $R_{ij}^{\text{ext}}(t)$ and the exciting force $F_j^{\text{ext}}(t)$ of wave action, ensuring consistency between the time steps of the external and internal fields. Finally, the numerical simulation terminates when $t > t_{\text{end}}$, where t_{end} indicates the preset end time.

2.3 Numerical validation

A comparison between the ship motion response from experimental data and hybrid numerical results is carried out to validate the reliability of the numerical model. The dimensions and parameter settings of the numerical model were maintained in the experiments. Initially, the roll motion response of an empty ship for three draught conditions was simulated, and the results are shown in Figure 6. The comparison indicates that the numerical results align well with the experimental data, suggesting that the potential flow-based numerical model effectively simulates the

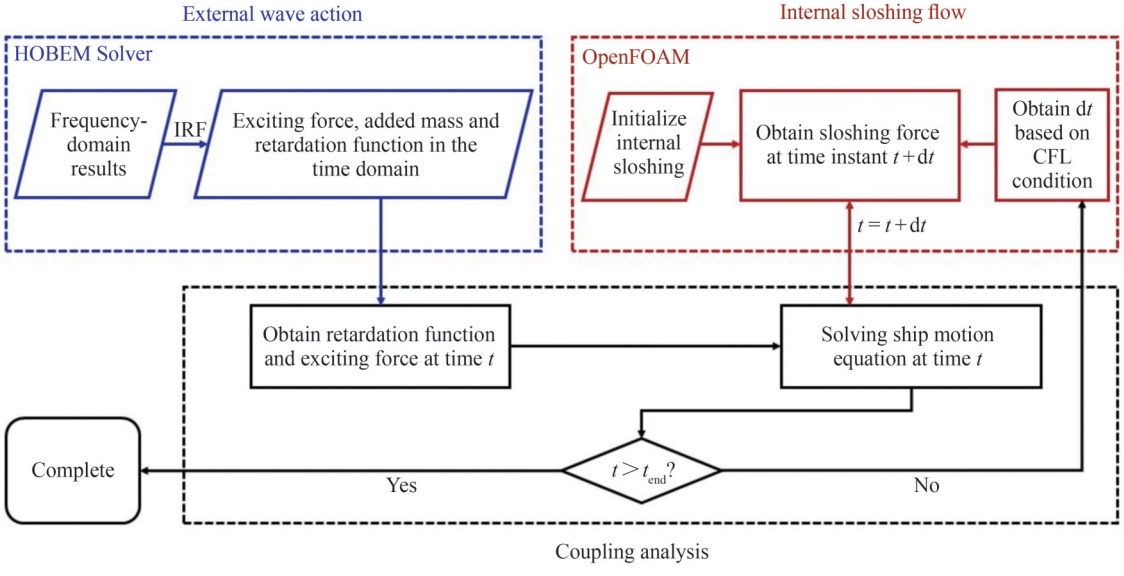

Figure 5 Illustration of the coupling between ship motion and liquid tank sloshing

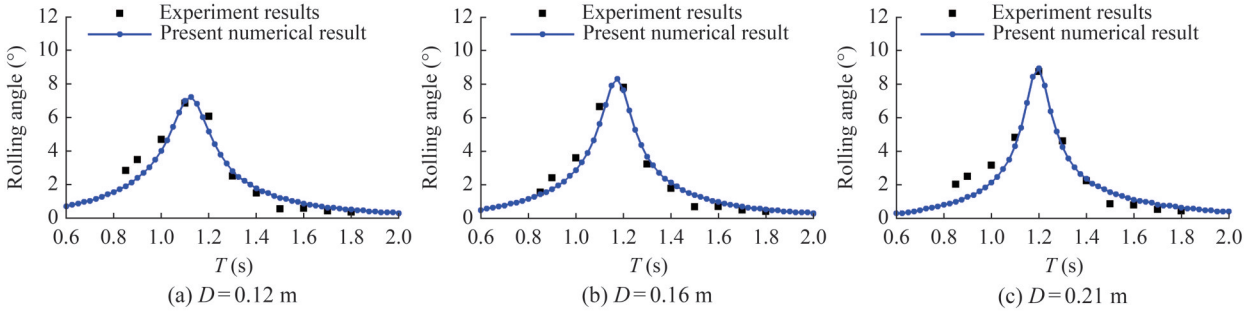

Figure 6 Validation of ship roll motion without sloshing

external wave action on the ship. For external linear wave action, the linear potential flow model provides satisfactory results. However, when significant nonlinearities in the external waves occur (e.g., wave breaking and narrow gap resonance), the linear potential flow model may no longer be adequate. In the future, external nonlinear potential flow models can be developed to address problems involving wave nonlinearities.

Furthermore, as shown in Figure 7, the roll motion amplitudes of the LNG ship with two prismatic tanks under regular wave action were simulated for three filling conditions. In general, the numerical results are in good agreement with the experimental data. A more detailed comparison reveals that medium filling (40%) and deep filling (60%) exhibit better conformity with the experimental results than shallow filling (20%). Shallow filling is more susceptible to complex nonlinear phenomena, such as breaking and splashing, which may explain the slightly larger discrepancy observed in this case. The internal viscous fluid model was validated in our previous work (Jiang et al., 2015) by comparing it with the experimental and numerical data of Liu and Lin (2009). The validation showed that the numerical model is accurate in solving sloshing problems, including wave resonance and surface breaking. This comparison further confirms that the hybrid numerical model is effective in simulating the coupling of ship roll motion and liquid sloshing under wave action.

Mesh convergence analysis was carried out on the numerical model for the three filling conditions. The internal fluid domain mesh was non-uniform, with refinement near the free surface and wall. Four mesh schemes were applied for each filling condition, as shown in Table 2. The incident wave amplitude was A = 0.050 m, and the wave period was the peak period shown in Figure 7. Figures 8(a)–(c) present the comparison of the ship roll motion response under the four mesh schemes. The figures evidently show that the results of Mesh 3 and Mesh 4 are very close to each other, indicating that Mesh 3 satisfies the convergence requirements. Therefore, to enhance computational efficiency while maintaining computational accuracy, Mesh 3 was selected for further numerical analysis.

3 Numerical results and discussion

The difference in ship motion responses between coupling LNG sloshing and coupling water sloshing inside under wave action was numerically investigated. The same LNG ship model was used in this study, with the model configurations for filling LNG and water shown in Table 3. The LNG filling consisted of four tanks, arranged consistent with that of the two water tanks. In this work, the density of LNG was selected as ρ_{LNG} = 499.1 kg/m^3 (ρ_{LNG} = 1/2ρ_{water}), and the kinematic viscosity was 1.2 × 10^{-7} m^2/s. This condition ensured that the basic parameters, such as the center of gravity, draft, and inertia of the ship with LNG and water fillings, were consistent. The ship was subjected to beam waves with two incident wave amplitudes (A = 0.025 and 0.050 m), and the incident wave period ranges from 0.50 s to 2.00 s, including the natural period of the ship roll motion

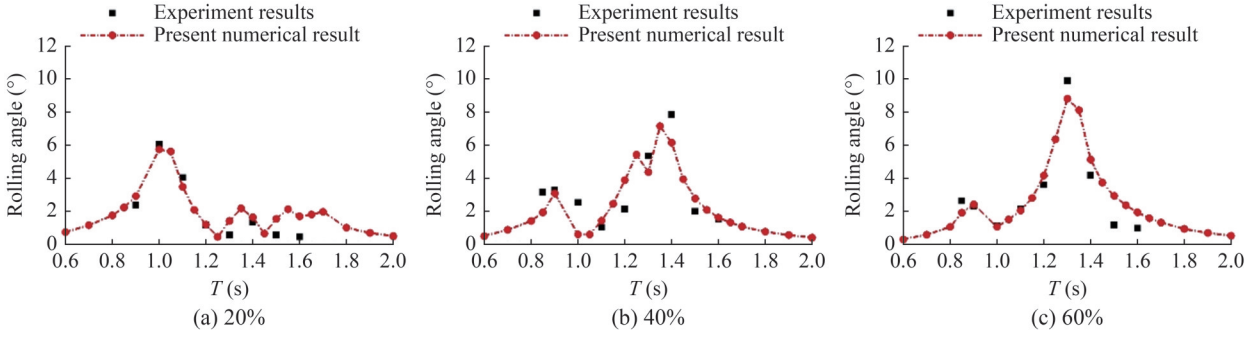

Figure 7 Validation of ship roll motion coupled with sloshing

Table 2 Mesh resolution for different mesh schemes

Filling condition (%)	Mesh 1	Mesh 2	Mesh 3	Mesh 4
20	20 520	44 892	85 608	182 664
40	25 920	54 000	100 800	208 800
60	33 696	63 000	120 960	252 000

for each filling condition. Three filling conditions (20%, 40%, and 60%) were considered.

3.1 Comparison of ship roll motion

Figures 9 and 10 show the comparison of ship rolling amplitudes (stead-state stage) between the "Empty" results, water and LNG filling results for incident wave amplitudes A = 0.025 and 0.050 m, respectively. A single-peak variation in ship roll motion amplitudes with incident wave periods is observed in the "Empty" results, whereas two-peak variations appear in the water and LNG filling results. This finding implies the significant influence of internal sloshing on the ship's roll motion responses in beam seas. Further comparisons reveal nearly identical ship roll motion amplitudes between the water and LNG filling results, suggesting that liquid type has an insignificant effect on the coupled ship roll motion response in beam seas, provided the total liquid mass is the same. Differences

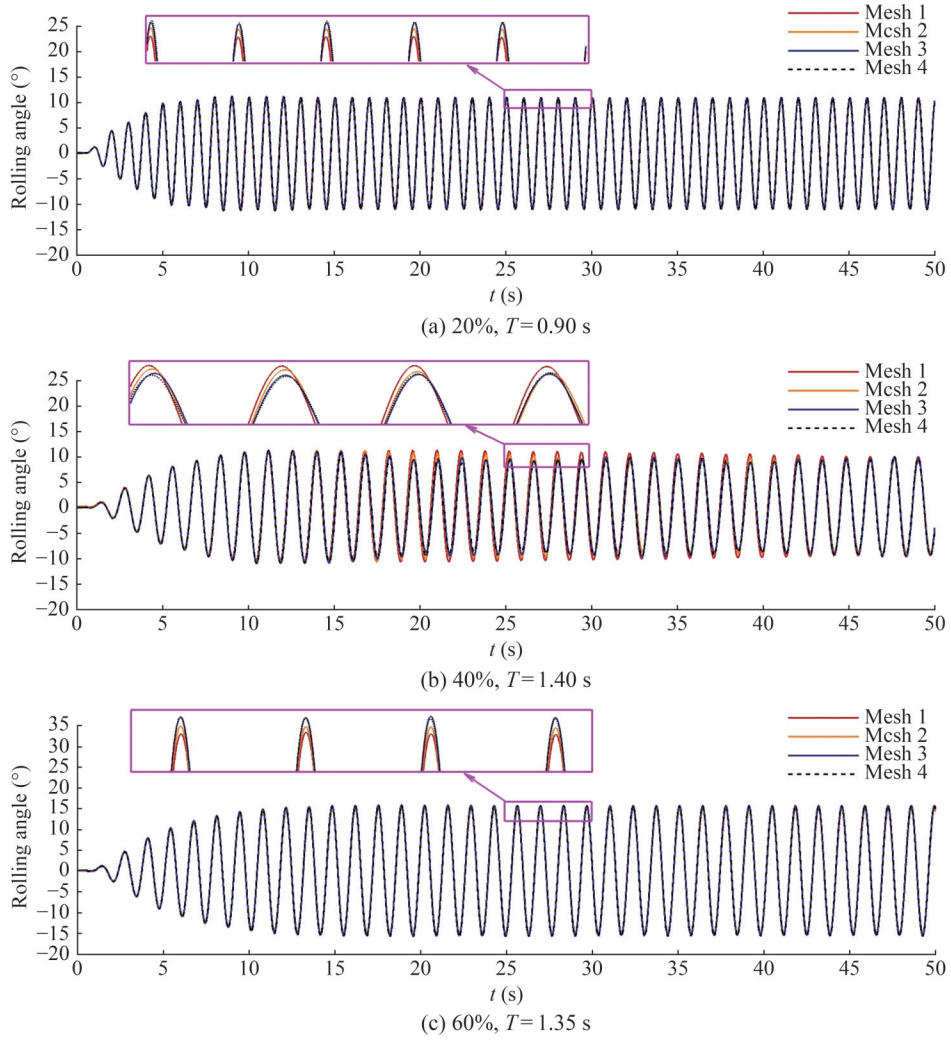

Figure 8 Time histories of ship roll motion at incident wave amplitude A = 0.05 m

Table 3 Comparison of tank configurations between LNG and water filling

	Number of tanks	Length of tanks (m)	Width of tanks (m)	Height of tanks (m)	Density (kg/m^3)	Kinematic viscosity (m^2/s)	Total liquid mass (kg)		
							20%	40%	60%
LNG	4	0.50	0.56	0.37	499.1	1.2×10^{-7}	39.28	80.72	122.16
Water	2				998.2	1.0×10^{-6}			

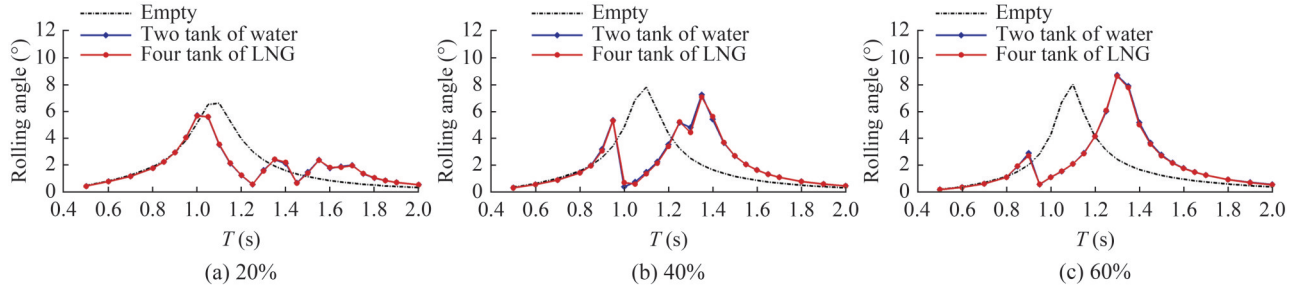

Figure 9 Comparison of ship roll motion coupled with filling-LNG sloshing and filling-water sloshing at incident wave amplitude $A = 0.025$ m

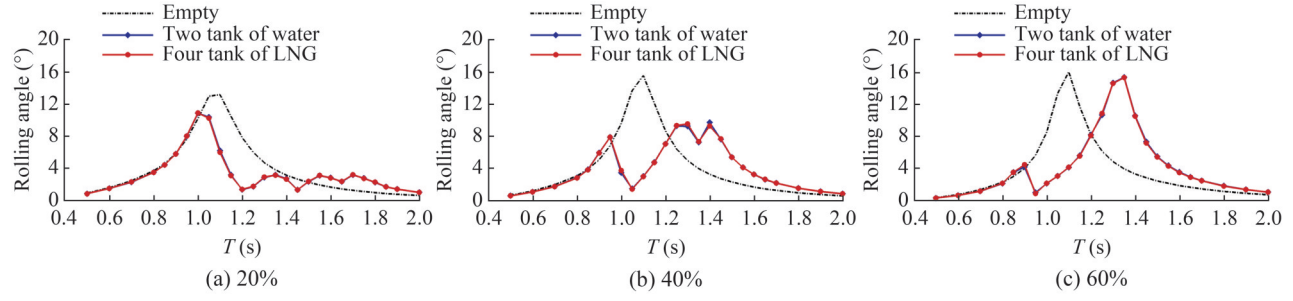

Figure 10 Comparison of ship roll motion coupled with LNG and water sloshing fillings at an incident wave amplitude $A = 0.050$ m

in the violent internal sloshing flow patterns are observed between the water and LNG filling cases, such as at the period $T = 1.30$ s under the 20% filling condition, which will be explained in Section 3.2. However, no essential discrepancy is found in the ship roll motion responses between the water and LNG filling results. In summary, water can reliably substitute LNG in experiments studying the motion response of LNG ships under beam wave action.

3.2 Comparison of point pressure

To assess the effects of water and LNG sloshing fillings on local impact loading on the tank, point pressures on the tank walls were considered. The point pressures at the free surface (P1), bilge chamfer (P2), and top chamfer (P3) were monitored, as shown in Figure 11. Three typical time signals of internal point pressure are illustrated in Figure 12, with corresponding snapshots of the internal flow and pressure fields shown in the two rightmost columns. As shown in Figure 12(a), the time signals of pressure exhibit a smooth pattern, and the sloshing flow follows a non-breaking pattern, referred to as Type 1. It occurs when the incident wave period is away from the corresponding periods of the two peak values of ship roll motion amplitudes. Around the peak period of the roll motion, the time signals of pressure display double-peak characteristics. As shown in Figure 12(b), the amplitudes of the pressure signals are nearly the same at the steady-state stage, with no impulsive characteristic in the time signals. By contrast, Figure 12(c) shows pressure signals with different amplitudes and distinct impulsive characteristics. The discrepancy in the pressure time signals is mainly due to the varying levels of breaking and splashing phenomena in the sloshing flow patterns in Figures 12(b) and (c), which are correspondingly defined as Type 2 and Type 3, respectively. More detailed characteristics of the three types of pressure signals are presented in Table 4. In addition, in the subsequent analysis, the average peak refers to the average of the larger peaks (between the pink dashed lines) of the pressure signal from 30 s to 50 s, whereas the pressure maximum represents the maximum value of the pressure signal.

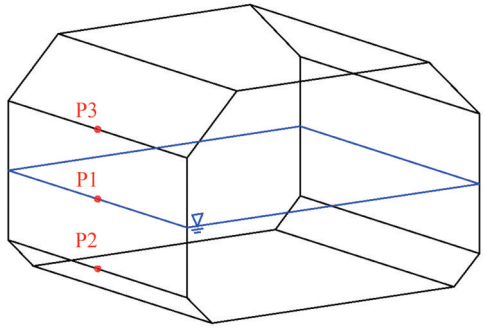

Figure 11 Location of pressure measurement points inside the tank

Figure 13 shows the average values of the pressure at point P1 for different filling conditions, with normalized pressure values of $A_P^{\text{avg.}}/\rho g A$ adopted. The discrepancy between water and LNG filling results is not evident. A slight difference can be observed in Figures 13(d) and (e), where the pressure signal types are Type 2 and Type 3. These results suggest that the breaking sloshing flow is the primary reason for the discrepancy in sloshing pressure behavior between the water and LNG filling cases. With the increase in incident wave amplitudes or the decrease in filling ratios, the discrepancy between water and LNG fillin-

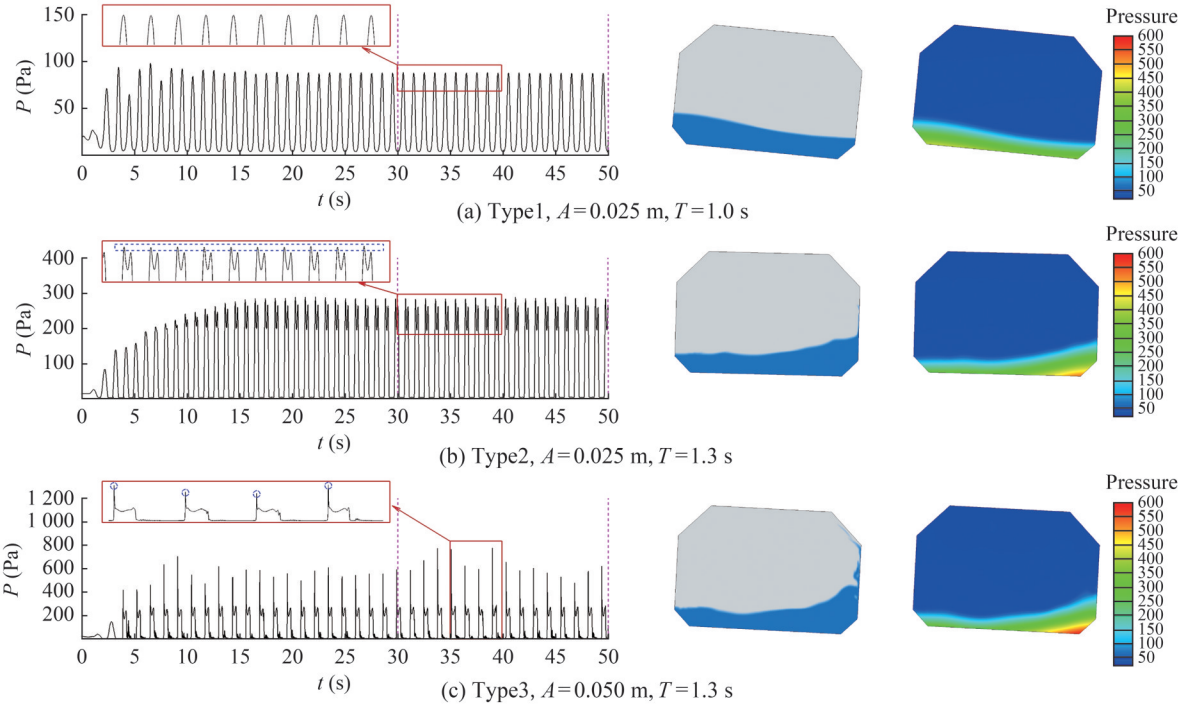

Figure 12 Time signals of the pressure for 20% filling condition

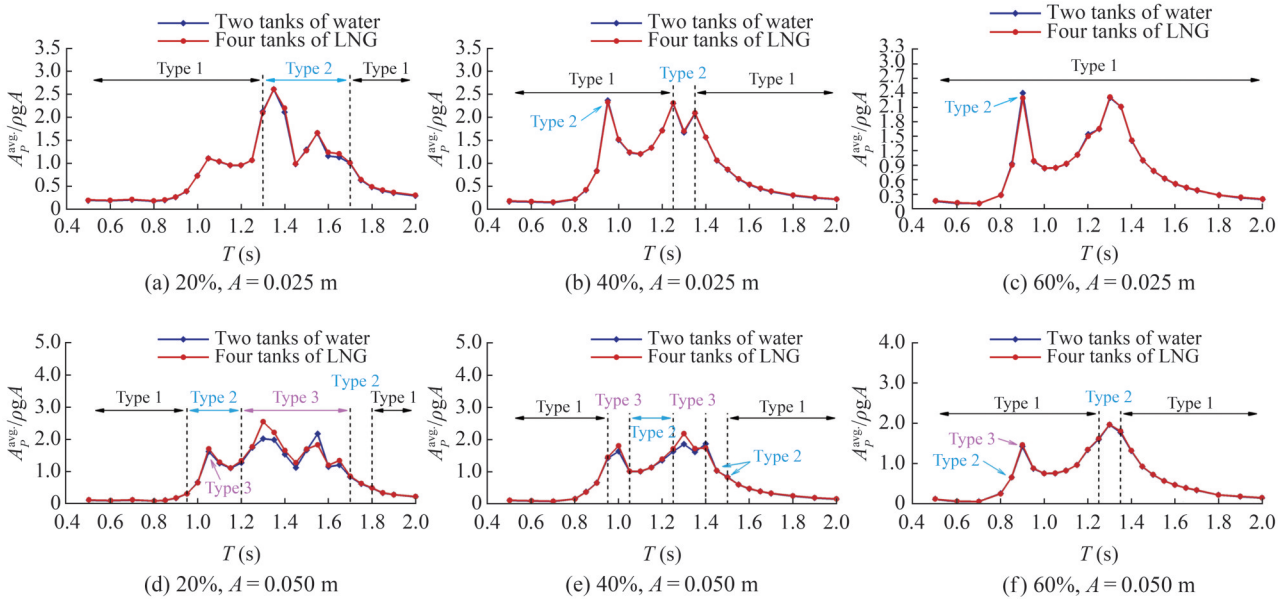

Figure 13 Comparison of average peak pressure at P1

Table 4 Definitions of different types of variations in internal pressure signals

Name	Wave amplitude	Periods	Position	Characteristic
Type 1	0.025 m, 0.050 m	Away peak	P1, P2, P3	Smooth pressure curve with no sudden changes.
Type 2	0.025 m, 0.050 m	Near peak	P1, P2	Double peaked pressure curve without evident impulsive characteristics.
Type 3	0.050 m	Peak	P1, P2, P3	Double peaked pressure curve with evident impulsive characteristics.

gs increases. This finding is attributed to the increased nonlinearity of internal sloshing flow. Figure 14 presents the maximum values of pressure at point P1, with normalized pressure values $A_P^{\max}/\rho gA$ adopted. The analysis of average pressure in Figure 13 also applies to the maximal values shown in Figure 14. However, the discrepancy between the water and LNG filling results in Figure 14 is more pronounced than in Figure 13. This finding suggests

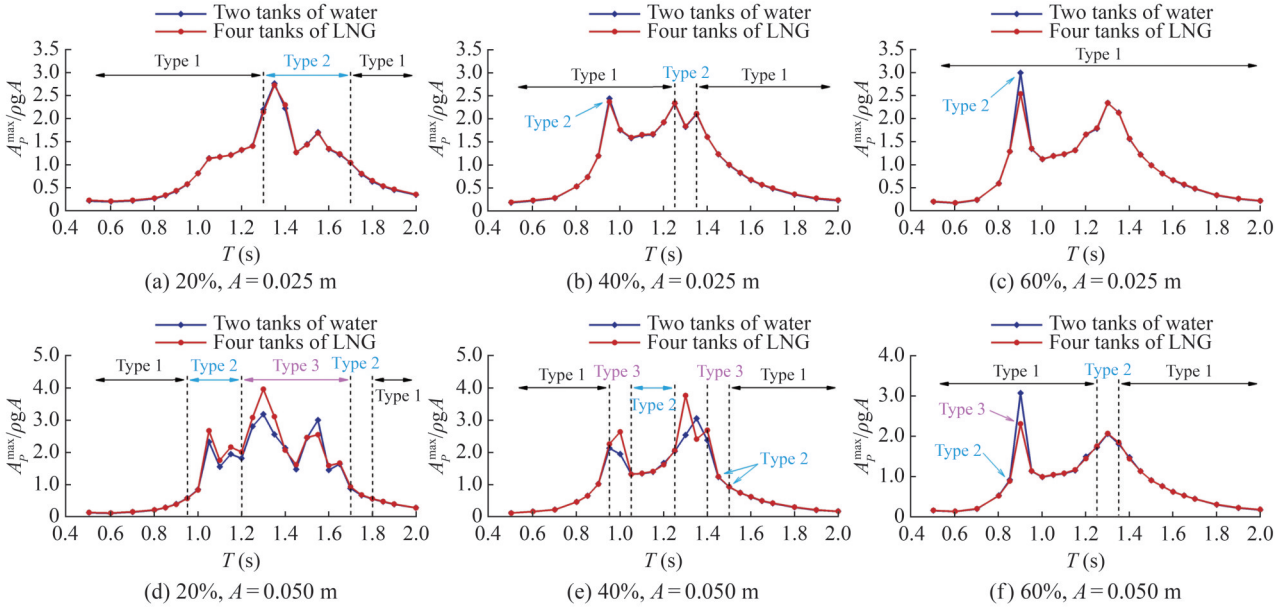

Figure 14 Comparison of pressure maximum at P1

that the influence of internal liquid sloshing on local impact loading exhibits random behavior. The normalized pressure values $A_P^{avg.}/\rho gA$ and $A_P^{max}/\rho gA$ are used in these figures. This finding implies the approximately twofold relationship when using water instead of LNG in experiments to study the internal pressure of LNG ships because the density of LNG is half that of water.

Furthermore, the pressure at point P2, located at the bilge chamfer, was statistically analyzed. The average and maximal peak pressures at point P2 are presented in Figures 15 and 16. The pressure time signal at point P2 follows the same pattern as that at point P1, demonstrating that the average peak pressure and maximum pressure at point P2 exhibit a similar pattern to point P1. When internal sloshing becomes violent and nonlinear phenomena such as overturning and breaking occur, the pressure signal shifts to Type 2 and Type 3. As a result, the pressures at point P2 for LNG and water fillings differ. In addition, a comparison of the pressure signals and internal snapshots for LNG and water fillings is shown in Figure 17. Although the pressure values differ due to variations in internal sloshing motion, the types of pressure signals for LNG and water fillings remain consistent. In general, the results suggest that using water instead of LNG to predict the pressure near the free surface and bottom of the tank introduces only slight bias, particularly when internal sloshing is violent.

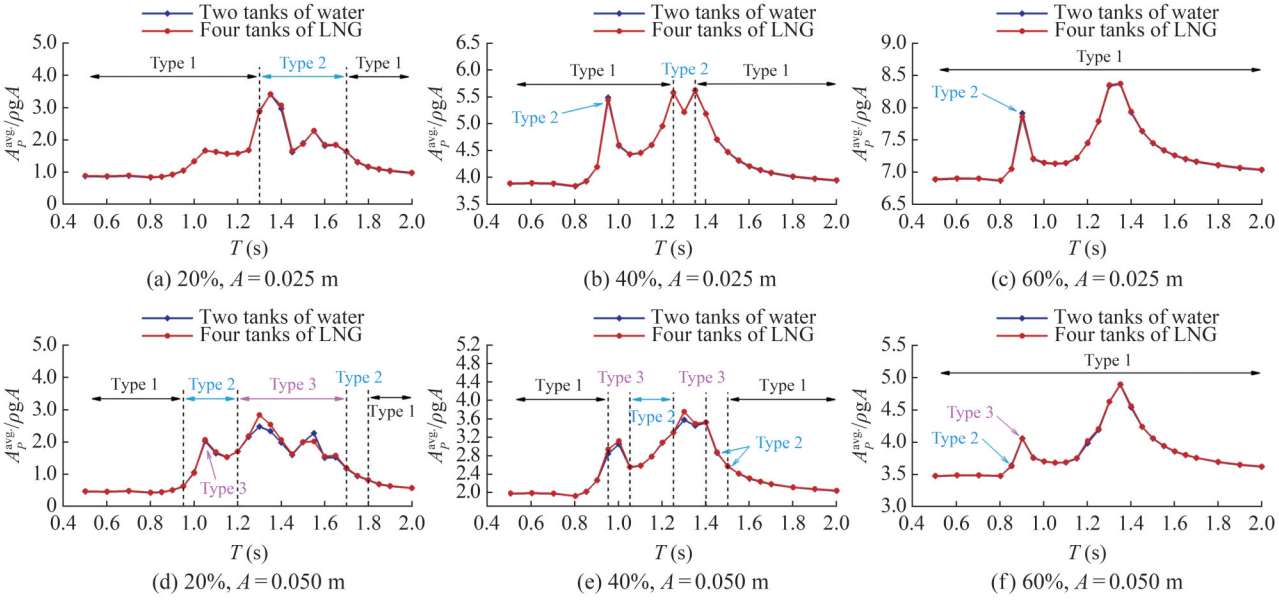

Figure 15 Comparison of average peak pressure at P2

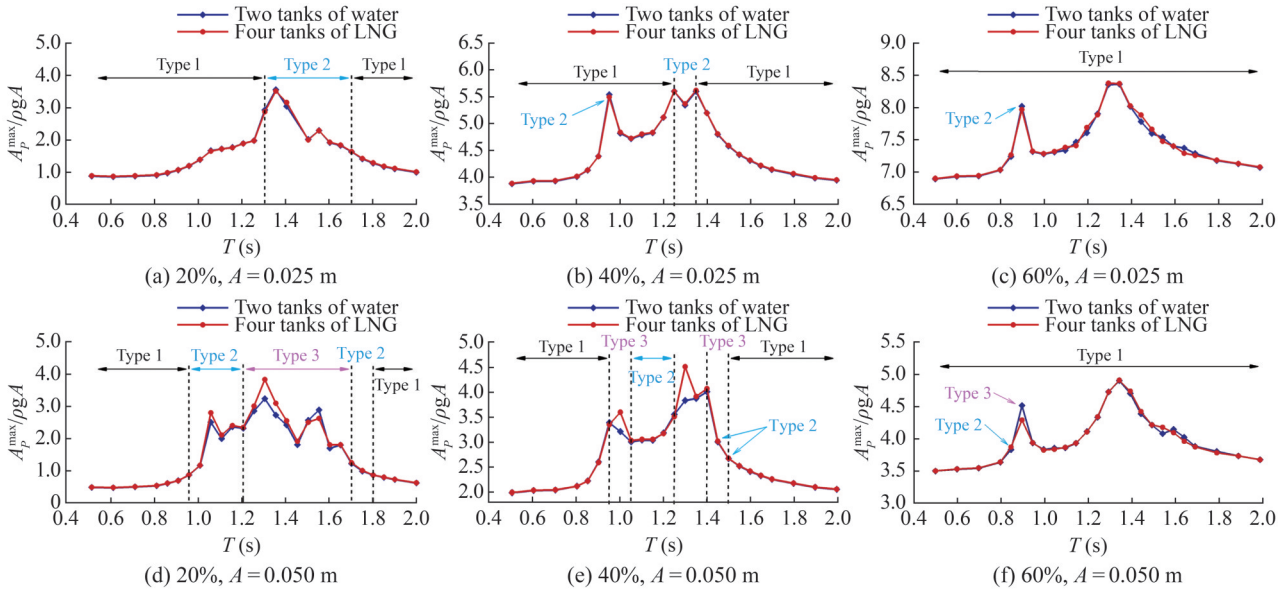

Figure 16 Comparison of pressure maximum at P2

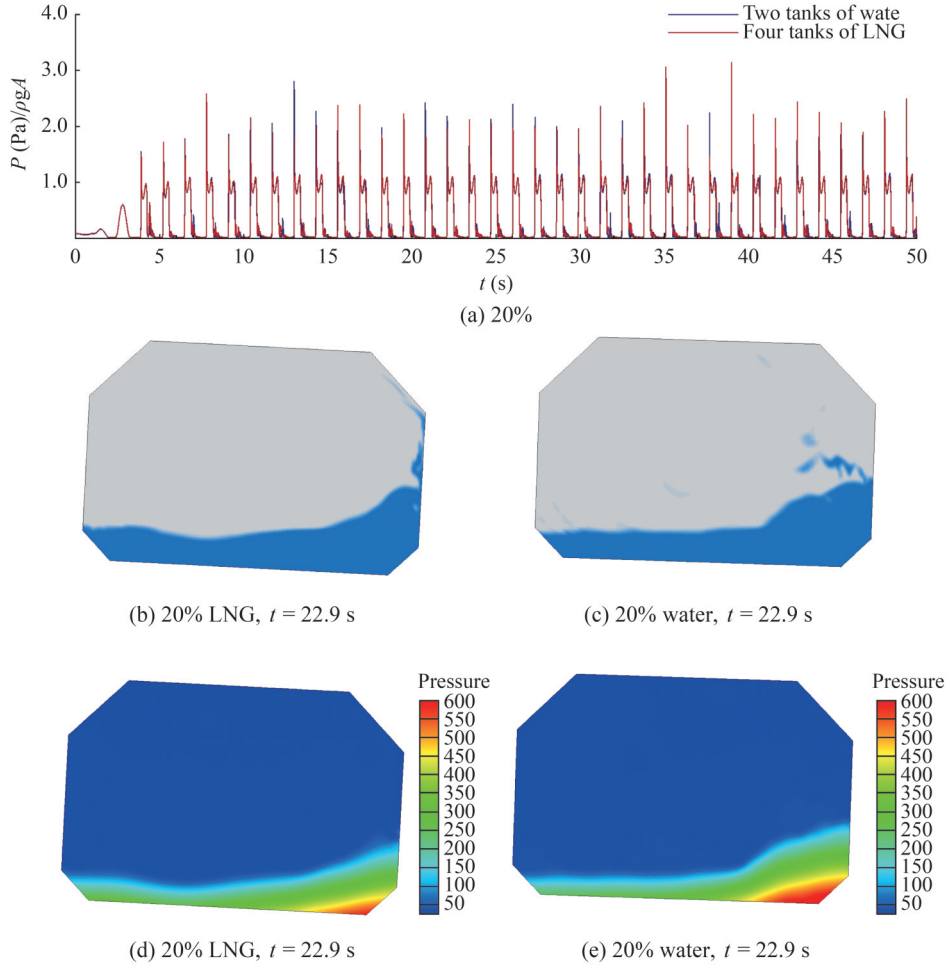

Figure 17 Comparison of internal pressure signals and snapshots for filling LNG and water at incident wave amplitude A = 0.050 m and period T = 1.3 s

Finally, the pressure at point P3, located at the tank top chamfer, was analyzed. As shown in Figure 18, the pressure signal at point P3 is mostly Type 3, exhibiting impulsive characteristics. This type of pressure is more likely to

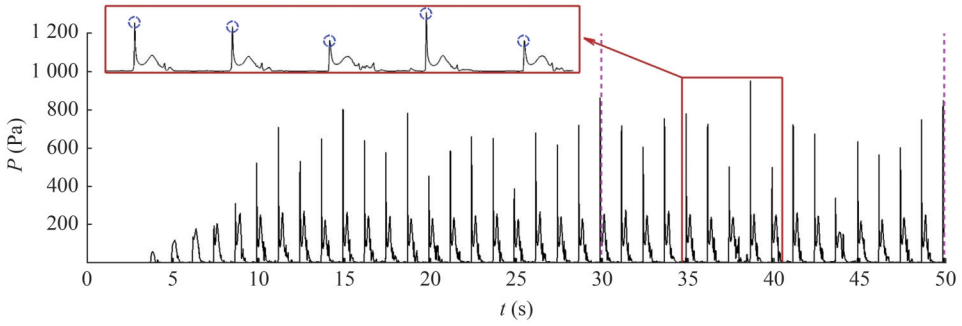

Figure 18 Time signals of the P3 pressure for 60% filling condition (A = 0.050 m, T = 1.25 s)

cause local damage to the internal structure of the tank, emphasizing the need for improved strength design of the prismatic tank top chamfer. Only the average peak pressure and maximum pressure between 30 s and 50 s for LNG and water fillings at point P3 with A = 0.050 m are provided in Figures 19 and 20 for the 40% and 60% filling conditions, given the little internal sloshing topping for small wave amplitude and shallow filling. For the 60% filling condition, the overall trends for LNG and water are similar, with noticeable differences occurring only at the peaks. However, the wider range of Type 3 pressure signatures at the 40% filling condition leads to remarkable differences between LNG and water. Moreover, this discrepancy is more pronounced in Figure 20 than in Figure 19. This finding indicates that the sloshing-induced pressure loads at the tank top chamfer exhibit a distinct random character. In general, although the difference in sloshing impact pressure between LNG and water filling results is minimal, using water in place of LNG in physical experiments provides reliable results.

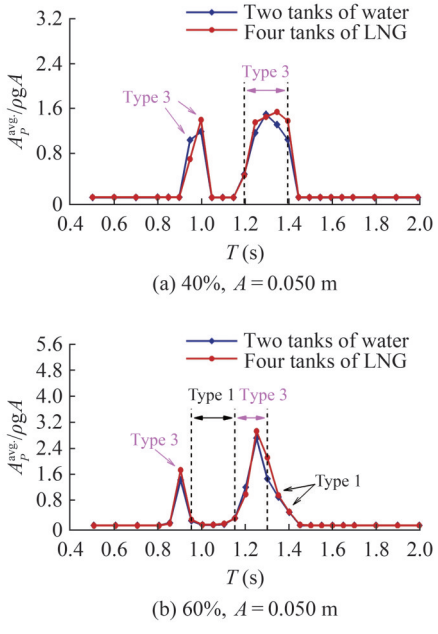

Figure 19 Comparison of average peak pressure at P3

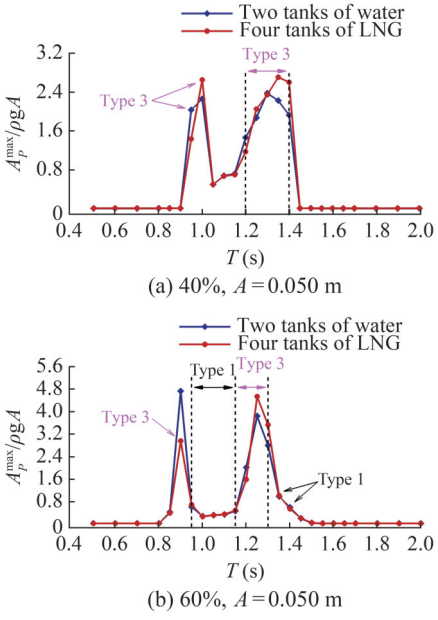

Figure 20 Comparison of pressure maximum at P3

4 Conclusion

In this study, a hybrid numerical model is used to investigate the coupling effect between floating body motion and liquid sloshing, where external wave action and internal sloshing flow are simulated using the potential flow model and viscous flow model, respectively. Comparisons of the ship roll motion response and internal sloshing pressure between LNG-filled tanks (four tanks) and water-filled tanks (two tanks) are conducted, with the total liquid mass maintained for both liquid types. The results show good agreement in ship roll motion response between LNG and water-filled tanks in beam sea conditions, indicating that water can reliably substitute LNG in experiments studying the motion response of LNG ships. Regarding the impact of liquid types on sloshing pressure, numerical simulations reveal minimal discrepancies in the average results between water and LNG-filled tanks, but differences are observed in the maximum values. Therefore, the maximum sloshing pressure obtained using water instead

of LNG should be further corrected through numerical simulation and other methods. However, a ρ_{LNG}/ρ_{water} relationship exists between the sloshing impact pressures of water and LNG, based on the density ratio of LNG to water. Thus, replacing LNG with water in physical experiments can provide reliable results for studying sloshing impact pressures.

Acknowledgement This work is supported by the Natural Science Foundation of China with Grant Nos. 52371267 and 52171250. The authors gratefully acknowledge the Supercomputer Center of Dalian University of Technology for providing computing resources.

Competing interest The authors have no competing interests to declare that are relevant to the content of this article.

Reference

Bouscasse B, Colagrossi A, Marrone S, Antuono M (2013) Nonlinear water wave interaction with floating bodies in SPH. Journal of Fluids and Structures 42, 112-129. DOI: 10.1016/j.jfluidstructs.2013.05.010

Cao X, Tao L, Zhang A, Ming F (2019) Smoothed particle hydrodynamics (SPH) model for coupled analysis of a damaged ship with internal sloshing in beam seas. Physics of Fluids 31, 032103. DOI: 10.1063/1.5079315

Chen X (2004) Hydrodynamics in offshore and naval applications-Part I. In: Presented at the 6th International Conference on HydroDynamics. The University of Western Australia, Perth, Australia

Cummins W (1962) The impulse response function and ship motions. In: Proceedings of the Symposium on Ship Theory, vol. 9. Hamburg, Germany, Schiffstechnik

Gaillarde G, Ledoux A, Lynch M (2004) Coupling Between Liquefied Gas and Vessel's Motion for Partially Filled Tanks: Effects on Seakeeping, In: Proceedings of the RINA Conference. London, UK

Gou Y, Kim Y, Kim T (2011) A Numerical Study on Coupling between Ship Motions and Sloshing in Frequency and Time Domains

He T, Feng D, Liu L, Wang X, Jiang H (2022) CFD Simulation and Experimental Study on Coupled Motion Response of Ship with Tank in Beam Waves. Journal of Marine Science and Engineering 10, 113. DOI: 10.3390/jmse10010113

Hu Z, Wang S, Chen G, Chai S, Jin Y (2017) The effects of LNG-tank sloshing on the global motions of FLNG system. International Journal of Naval Architecture and Ocean Engineering 9, 114-125. DOI: 10.1016/j.ijnaoe.2016.09.007

Huang S, Duan W, Han X, Nicoll R, You Y, Sheng S (2018) Nonlinear analysis of sloshing and floating body coupled motion in the time-domain. Ocean Engineering 164, 350-366. DOI: 10.1016/j.oceaneng.2018.06.003

Huang W, He T, Yu J, Wang Q, Wang X (2021) Direct CFD simulation and experimental study on coupled motion characteristics of ship and tank sloshing in waves, In: proceedings of the ASME 2021 40TH international conference on ocean, offshore and arctic engineering, Electr network

Jiang S, Teng B, Bai W, Gou Y (2015) Numerical simulation of coupling effect between ship motion and liquid sloshing under wave action. Ocean Eng 108, 140-154. https://doi.org/10.1016/j.oceaneng.2015.07.044

Jiang S, Bai W (2020) Coupling analysis for sway motion box with internal liquid sloshing under wave actions. Physics of Fluids 32, 072106. DOI: 10.1063/5.0015058

Jiao J, Ding S, Zhao M, Jiang M, Bu S, Shi Y (2024a) Simulation of LNG ship's motions coupled with tank sloshing in regular waves by DualSPHysics. Ocean Engineering 312, 119148. DOI: 10.1016/j.oceaneng.2024.119148

Jiao J, Zhao M, Jia G, Ding S (2024b) SPH simulation of two side-by-side LNG ships' motions coupled with tank sloshing in regular waves. Ocean Engineering 297, 117022. DOI: 10.1016/j.oceaneng.2024.117022

Lee S, Kim M (2010) The Effects of Inner-Liquid Motion on LNG Vessel Responses. Journal of Offshore Mechanics and Arctic Engineering 132, 021101. DOI: 10.1115/1.4000391

Li Y, Su M, Li H, Deng R, Wang K, Hu Z (2019) Numerical research on time domain ship motions coupled with sloshing at different liquid levels and forward speeds. Ocean Engineering 178, 246-259. DOI: 10.1016/j.oceaneng.2019.02.063

Liu L, Feng D, Wang X, Zhang Z, Yu J, Chen M (2022) Numerical study on the effect of sloshing on ship parametric roll. Ocean Engineering 247, 110612. DOI: 10.1016/j.oceaneng.2022.110612

Liu D, Lin P (2009) Three-dimensional liquid sloshing in a tank with baffles. Ocean Eng 36, 202-212. https://doi.org/10.1016/j.oceaneng.2008.10.004

Lyu W, Moctar O, Schellin T (2022) Ship motion-sloshing interaction with forward speed in oblique waves. Ocean Engineering 250, 110999. DOI: 10.1016/j.oceaneng.2022.110999

Molin B (2002) "LNG-FPSO's: Frequency domain, coupled analysis of support and liquid cargo motion", in Proceedings of the IMAM conference, Rethymnon, Greece

Nam B, Kim Y, Kim D, Kim Y (2009) Experimental and Numerical Studies on Ship Motion Responses Coupled with Sloshing in Waves. Journal of Ship Research 53, 68-82

Newman J (2005) Wave effects on vessels with internal tanks. Spitsbergen. In: Proceedings of the 20th Workshop on Water Waves and Floating Bodies. Spitsbergen, Norway

Rognebakke O, Faltinsen O (2003) Coupling of Sloshing and Ship Motions. Journal of Ship Research 47, 208-221

Saripilli J, Sen, D (2018) Numerical studies on effects of slosh coupling on ship motions and derived slosh loads. Applied Ocean Research 76, 71-87

Su Y, Liu Z (2017) Coupling effects of barge motion and sloshing. Ocean Engineering 140, 352-360. DOI: 10.1016/j.oceaneng.2017.06.006

Teng B, Taylor R (1995) New higher-order boundary element methods for wave diffraction/radiation. Applied Ocean Research. 17, 71-77

Tabri K, Matusiak J, Varsta P (2009) Sloshing interaction in ship collisions—An experimental and numerical study. Ocean Engineering 36, 1366-1376. DOI: 10.1016/j.oceaneng.2009.08.017

Wang J, Sun S, Hu J (2017) The coupling analysis of tank motion and sloshing by a fully nonlinear decoupling method. Nonlinear Dynamics 89, 971-985. DOI: 10.1007/s11071-017-3495-0

Zhang Z, Wu Q, Xie Y, Yu H (2023) Experimental and numerical investigations on the liquid tank sloshing in regular waves. Ocean Engineering 271, 113668. DOI: 10.1016/j.oceaneng.2023.113668

Zhao W, Taylor P, Wolgamot H, Eatock Taylor R (2018) Identifying linear and nonlinear coupling between fluid sloshing in tanks, roll of a barge and external free-surface waves. J. Fluid Mech. 844, 403-434. DOI: 10.1017/jfm.2018.186

Zhao W, Yang J, Hu Z, Tao L (2014a) Coupling Between Roll

Motions of an FLNG Vessel and Internal Sloshing. Journal of Offshore Mechanics and Arctic Engineering 136, 021102. DOI: 10.1115/1.4026586

Zhao W, Yang J, Hu Z, Xiao L, Tao L (2014b) Hydrodynamics of a 2D vessel including internal sloshing flows. Ocean Engineering 84, 45-53. DOI: 10.1016/j.oceaneng.2014.03.001

Zhao W, Yang X, Wan D (2024) Numerical analysis of coupled sloshing and motion of a cylindrical FPSO in regular waves. Journal of Hydrodynamics 36, 457-465. DOI: 10.1007/s42241-024-0032-8

Zheng M, Ni Y, Wu C, Jo H (2021) Experimental investigation on effect of sloshing on ship added resistance in head waves. Ocean Engineering 235, 109362. DOI: 10.1016/j.oceaneng.2021.109362

Zhu Z, Lee J, Kim Y, Lee J, Park T H (2021) Experimental measurement and numerical validation of sloshing effects on resistance increase in head waves. Ocean Engineering 234, 109321. DOI: 10.1016/j.oceaneng.2021.109321

Zhuang Y, Wan D (2019) Numerical Study on Ship Motion Fully Coupled with LNG Tank Sloshing in CFD Method. International Journal of Computational Methods 16, 1840022. DOI: 10.1142/S0219876218400224

Zhuang Y, Wang G, Wan D, Wu J (2022) Numerical simulations of FPSO with sloshing tanks in a random freak waves. Journal of Hydrodynamics 34, 491-498. DOI: 10.1007/s42241-022-0036-1